RSC Advances

PAPER

View Article Online
View Journal | View Issue

Cite this: *RSC Adv.*, 2017, **7**, 47297

Development of a series of bis-triazoles as G-quadruplex ligands†

Maysaa M. Saleh, [ac] Charles A. Laughton, [a] Tracey D. Bradshaw [a] and Christopher J. Moody *[b]

Maintenance of telomeres – specialized complexes that protect the ends of chromosomes – is provided by the enzyme complex telomerase, which is a key factor that is activated in more than 80% of cancer cells, but absent in most normal cells. Targeting telomere maintenance mechanisms could potentially halt tumour growth across a broad spectrum of cancer types. Telomeric ends of chromosomes consist of noncoding repeat sequences of guanine-rich DNA. These G-rich ends can fold into structures called G-quadruplexes. Stabilization of G-quadruplexes by small binding molecules called G4 ligands can prevent telomerase enzyme from maintaining telomere integrity in cancer cells. G-quadruplexes can exist in other parts of the genome too, especially within promoter sequences of oncogenes, and also be interesting drug targets. Here, we describe the development of a new series of novel bis-triazoles, designed to stabilize G-quadruplex structures selectively as G4 ligands. FRET assays showed two compounds to be moderately effective G4 binders, with particular affinity for the quadruplex formed by the Hsp90a promoter sequence, and good selectivity for G-quadruplex DNA *vs.* duplex DNA. However, CD spectroscopy failed to provide any information about the folding topology of the human telomeric G-quadruplex resulting from its interaction with one of the ligands. All the new ligands showed potent cell growth inhibitory properties against human colon and pancreatic cancer cell lines, as evidenced by the MTT assay; notably, they were more potent against cancer cells than in fetal lung fibroblasts. Docking studies were performed to rationalize the affinity of these ligands for binding to the telomeric parallel G-quadruplex DNA.

Received 30th June 2017
Accepted 8th September 2017

DOI: 10.1039/c7ra07257k

rsc.li/rsc-advances

Introduction

In eukaryotes, the ends of chromosomes are protected by telomeres, the specialized protein–DNA complexes that prevent end-to-end fusions, recombination and damage to the genome.[1] In humans, telomeres consist of the sequence (5′-GGGTTA-3′), which is referred to as the "telomeric repeat".[2] These repeating sequences are predominantly double-stranded. However there is an overhanging single-stranded G-rich 3′-end, known as 3′-overhang or G-strand, which plays an important structural and functional role.[3] Each chromosome end contains approximately 1000 to 2000 telomeric repeats.[2] In human somatic cells, telomere length decreases with each cell division event until it reaches a critical level, at which point cell division ceases, preventing loss of vital chromosomal genetic information.[4,5] Telomeres are replenished by an enzyme called telomerase, a "ribonucleoprotein complex" that functions as a reverse transcriptase to add multiple copies of (5′-GGGTTA-3′) – in all vertebrates – to the end of the G-strand of the telomere. Human telomerase consists of two main components: a protein called hTERT (human telomerase reverse transcriptase) and an RNA (3′-CAAUCCCAAUC-5′) known as hTR (human telomerase RNA) or hTERC (human telomerase RNA component). The protein hTERT uses hTERC to add a six-nucleotide repeating sequence (5′-GGGTTA-3′) to the 3′ G-strand of chromosomes.[6,7] A number of studies has revealed that telomerase activity is almost absent in normal somatic cells. However, a low level of telomerase activity has been discovered in mitotically active cells, including skin, lymphocytes, and endometrium because telomerase activity in these proliferating cells is regulated by growth. But in >80% cancers, tumour cells possess short telomeres and high levels of telomerase activity.[3] For this reason, most telomere-related anti-tumour strategies target the telomerase enzyme by which telomere maintenance is provided; the inhibition of telomerase activity results in the reduction of telomere length, and ultimately delayed cell death and abrogation of tumorigenicity *in vivo*.[6]

The telomeric DNA G-strand folds to form G-quadruplexes, also known as G4-DNA, which are four stranded structures

[a]*School of Pharmacy, Centre of Bimolecular Science, University of Nottingham, University Park, Nottingham NG7 2RD, UK*

[b]*School of Chemistry, University of Nottingham, University Park, Nottingham NG7 2RD, UK. E-mail: c.j.moody@nottingham.ac.uk*

[c]*Faculty of Pharmacy, Isra University, Queen Alia Airport Road, Amman 11 622, UK*

† Electronic supplementary information (ESI) available: Chemistry experimental protocols, copies of CD spectra, copies of LC-MS data for the tested compounds **44–53**, ^{1}H and ^{13}C NMR spectra for compounds **34–53**. See DOI: 10.1039/c7ra07257k

formed by nucleic acid sequences which are rich in guanine (Fig. 1). Each structure contains several stacked square arrangements of guanines called G-quartets.[8] Each G-quartet is composed of four guanines held together by a cyclic arrangement of eight hydrogen bonds. The presence of a central monovalent cation (typically potassium) helps to maintain the stability of the structure.[6,9,10]

Two principal categories of G-quadruplex nucleic acids have received attention as potential therapeutic targets: (i) those capable of being formed at the single-stranded G-overhang of telomeric DNA, for which appropriate small molecule ligands can induce G-quadruplex formation, stabilize its structure, inhibit telomerase activity and telomere elongation, and selectively target telomere maintenance, (ii) those within genomes, especially within promoter sequences of genes involved in cellular proliferation and oncogenes such as *c-myc*, *c-kit*, and Hsp90. It has been suggested that ligands that bind selectively with promoter G-quadruplexes could in principle down-regulate the expression of these genes and thus have an anticancer effect.[11,12] The G-quadruplex stabilization occurs, in most cases, *via* π–π staking and electronic interactions resulting in binding of the ligand on the G-quartet of the external face of the G-quadruplex (external stacking).[13] A wide range of small molecules such as BRACO-19,[14] telomestatin,[15] RHPS4,[16] MMQ_3,[17] Mn(III)-porphyrin,[18] BMSG-SH-3,[12] and TRZ,[1,19] have been investigated as G-quadruplex binding and stabilizing ligands (Fig. 2).

An efficient G-quadruplex ligand should feature; (i) a large aromatic flat surface, much larger than that of a duplex binder to improve the aromatic–aromatic overlap and provide selectivity, (ii) short alkyl chain substituents normally terminating in an amino group that is fully cationic at physiological pH. The positively charged amino groups improve the water-solubility of the ligand and create electrostatic interactions between the ligand and the G-quadruplex–DNA scaffold.[11,13]

We report here the design, synthesis, biophysical and biological evaluations, and molecular modeling studies of a new series of bis-triazoles, based upon a benzo[2,3-*d*, 5,6-*d*] ditriazolo-4,8-dione scaffold, which were developed to stabilize G-quadruplex structures selectively, as G4 ligands and experimental antitumour agents. We selected this scaffold for a number of reasons: firstly it features a novel planar G-quadruplex stacking moiety; secondly synthetic routes to the final compounds are highly convergent, quick, and flexible; and thirdly the symmetrical nature of the ligands potentially simplifies the analysis of their interactions with DNA.

Results and discussion

Synthetic chemistry

A new series of bis-triazoles were designed to display both hydrophobic and hydrophilic characteristics to bind to and stabilize G-quadruplex structures, as G4 ligands. The design

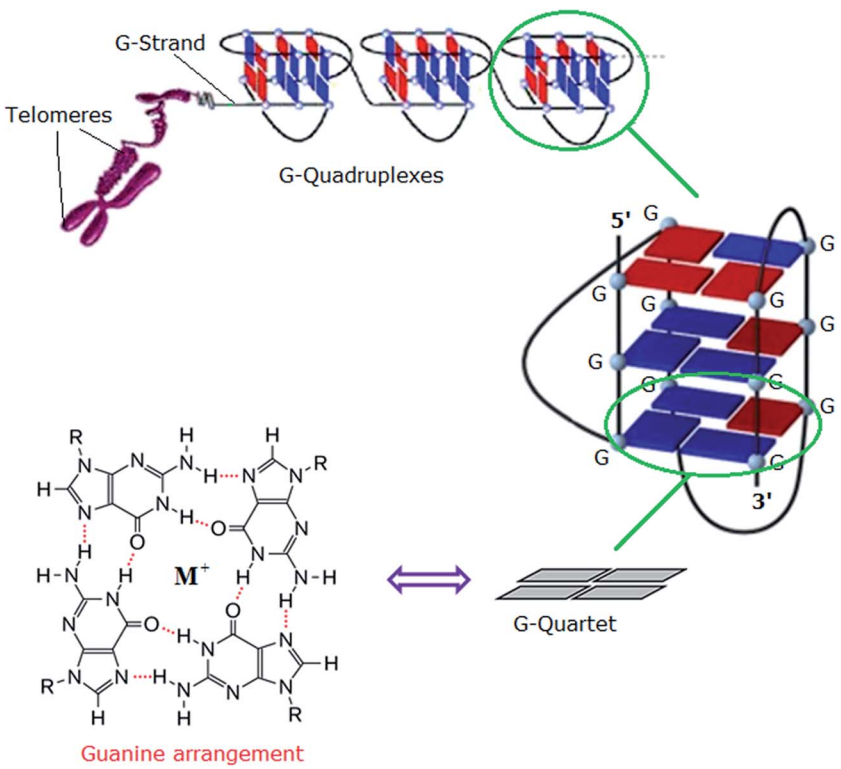

Fig. 1 Left: structure of a G-quartet involving four coplanar guanines with a central monovalent cation (guanine arrangement). Right: an intramolecular G-quadruplex. Blue and red boxes represent guanine bases in the *anti* and *syn* conformations, respectively.[6] Adapted from Y. Xu, T. Ishizuka, K. Kurabayashi, M. Komiyama, *Angew. Chem., Int. Ed.* 2009, **48**, 7833–7836. Copyright Wiley-VCH Verlag GmbH & Co. KGaA.[9] Reproduced with permission. And L.-P. Bai, M. Hagihara, K. Nakatani, Z.-H. Jiang, *Nature Sci. Rep*. DOI: 10.1038/srep06767, 2014.[10] Reproduced with permission from Nature Publishing Group.

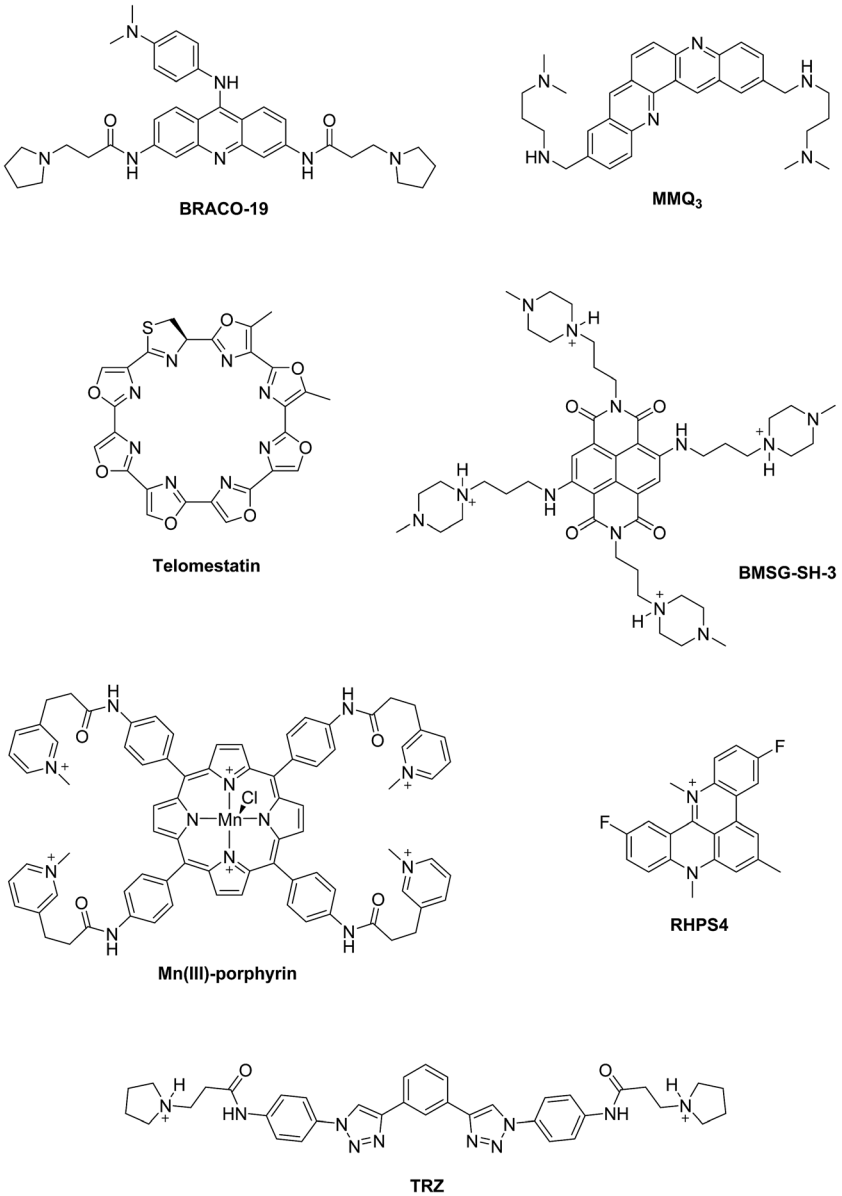

Fig. 2 Examples of G-quadruplex binding and stabilizing ligands reported in the literature.

included an aromatic core, represented by the bis-(benzyltriazolo)benzoquinone moiety, that promotes π-stacking with the G4 platform, and two protonatable side arms (amino groups) around the aromatic core. The positively charged amino groups are expected to improve the hydrophilicity of the ligands and create electrostatic interactions with the G4-grooves.

The synthesis of the hydrophobic aromatic core required a three-step process, as shown in Scheme 1. Heating the commercially available *p*-nitrobenzyl bromide **1** with sodium azide afforded *p*-nitrobenzyl azide **2** in yields of 82%.[20] 1,3-Dipolar cycloaddition reaction of **2** with benzoquinone **3** in the ratio 2 : 1 under reflux condition in ethyl acetate yielded 66% of bis-triazole **4**.[21–23] Bis-triazole core **5** was obtained in good yield (92%) by palladium catalyzed hydrogenation of **4** with hydrogen. ^{13}C NMR spectra for bis-triazoles **4** and **5** showed one peak for one carbonyl carbon which confirmed the symmetrical *trans*-regioisomer rather than *cis*-isomer that would show two different carbonyl signals.

A three-step route was followed to obtain the side chains **24–33** (Scheme 2). The halo esters **6a–d** were heated with secondary amines (diethylamine, morpholine and piperidine) to give the corresponding amino esters **7–13** in yields of 55–94%,[24] while the morpholine derivative **10** was commercially available. Conversion into the corresponding amino acids **14–23** was achieved by treating esters **7–13** with potassium hydroxide. Acids **14**, **19** and **20** were available commercially. Treating acids **14–23** with oxalyl chloride and a catalytic amount of DMF under an inert atmosphere produced the side chain acid chlorides **24–33**, which were used immediately for the next step.

The acid chlorides **24–33** were coupled successively to the hydrophobic aromatic core **5** in the presence of pyridine as a catalyst and under inert atmosphere to give novel compounds

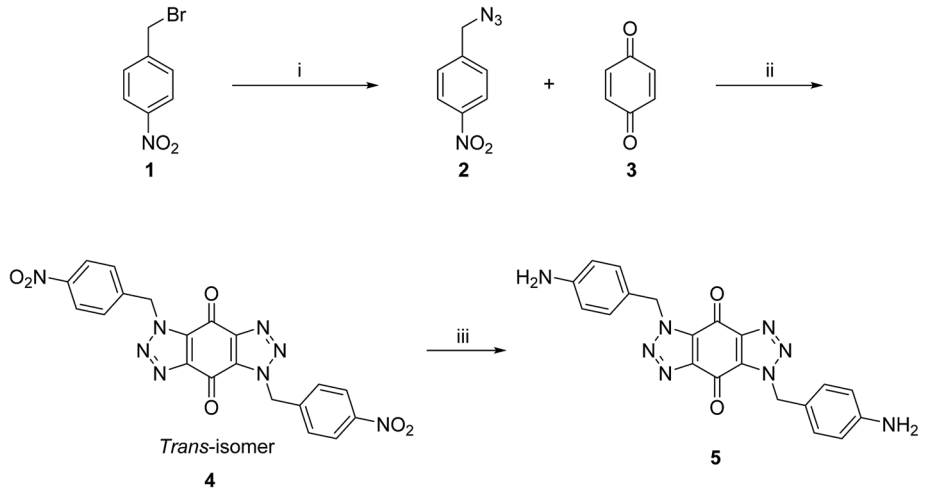

Scheme 1 Synthetic route for the aromatic core of bis-triazole **5**. Reagents and conditions: (i) NaN_3, acetone, reflux, 24 h, 82%; (ii) ethyl acetate, reflux, 48 h, 66%; (iii) H_2, Pd/C, DMF, rt, 4 h, 93%.

34–43 in yields of 38–90%. Treating amines **34–43** with hydrogen chloride in methanol solution, converted them into the corresponding hydrochloride salts **44–53** in good yields (65–95%), as shown in Scheme 3. The salts were purified either by trituration in hot methanol or recrystallization from methanol–light petroleum (1 : 1).

A mechanism is proposed in Scheme 4 for the formation of bis-triazole **4**. The first step is the 1,3-dipolar cycloaddition reaction of azide **2** with the activated C=C of *p*-benzoquinone **3** to produce the mono-triazoline intermediate **A** which is tautomerized and oxidized by the excess of **3** to form the mono-triazole adduct **C** derivative. A second 1,3-dipolar cycloaddition reaction and oxidation takes place in the same way to produce the *trans*-bis-triazole **4**.[21,22] The TLC analysis of the reaction mixture filtrates indicted the presence of excess organic azides and large amounts of hydroquinone which supports the proposal that excess benzoquinone plays the role of the required oxidant.

Binding to DNA

1. FRET assay. Bis-triazoles **44–53** were evaluated for their ability to bind and stabilize G-quadruplex DNA selectively by a FRET melting assay.[25–27] Four labeled oligomers were used: F21T is a G-quadruplex forming oligomer of the human telomeric sequence (5′-*FAM*-GGGTTAGGGTTAGGGTTAGGG-*TAMRA*-3′), *c-kit2* is a G-quadruplex forming oligomer of *c-kit2* oncogene (5′-*FAM*-CCCGGGCGGGCGCGAGGGAGGGGAGG-*TAMRA*-3′), Hsp90a is G-quadruplex forming oligomer of the promoter sequence of Hsp90a (5′-*FAM*-GGGCCAAAGGGAAGGGGTGGG-*TAMRA*-3′), and F10T (ds) is a hairpin double helix forming labelled oligomer

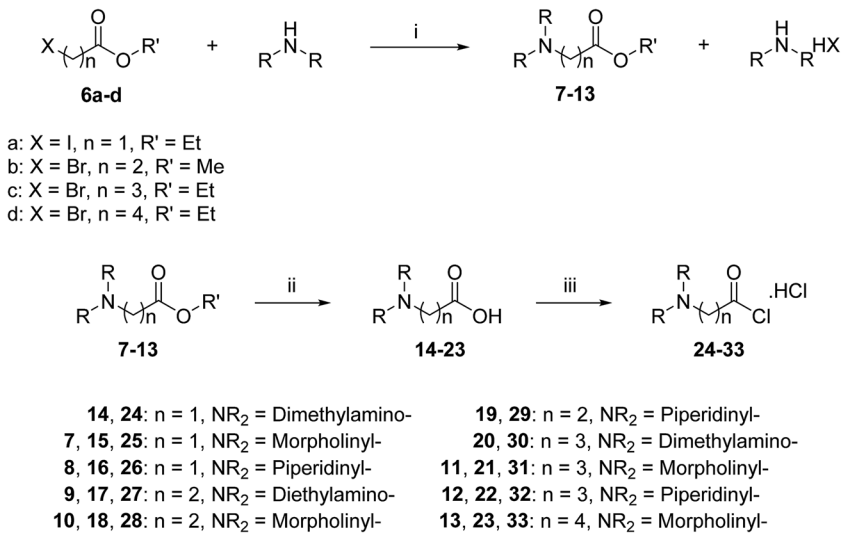

Scheme 2 General synthetic route for side chains **24–33**. Reagents and conditions: (i) acetonitrile, reflux, 2–8 h, 55–94%; (ii) (a) KOH, H_2O/ethanol or methanol, rt, 3–6 h, (b) 0.25 M HCl; (iii) oxalyl chloride, DMF, CH_2Cl_2, rt, 2–20 h.

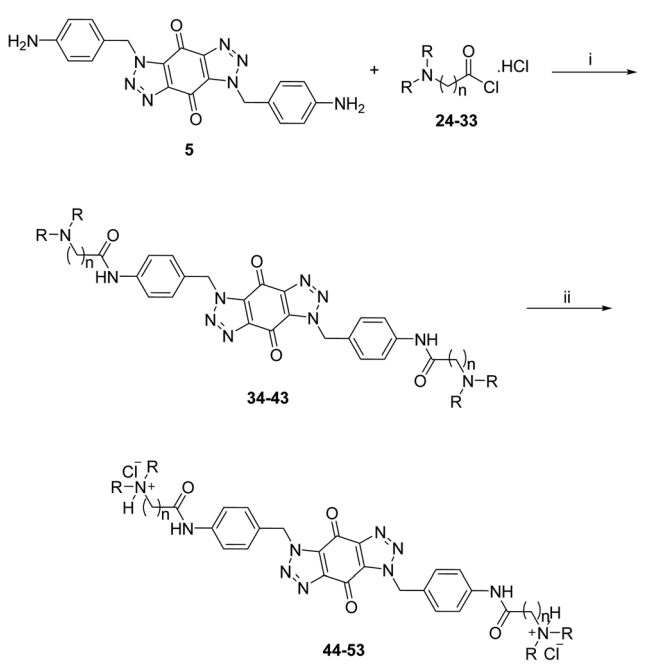

34, **44**: n = 1, NR_2 = Dimethylamino-
35, **45**: n = 1, NR_2 = Morpholinyl-
36, **46**: n = 1, NR_2 = Piperidinyl-
37, **47**: n = 2, NR_2 = Diethylamino-
38, **48**: n = 2, NR_2 = Morpholinyl-
39, **49**: n = 2, NR_2 = Piperidinyl-
40, **50**: n = 3, NR_2 = Dimethylamino-
41, **51**: n = 3, NR_2 = Morpholinyl-
42, **52**: n = 3, NR_2 = Piperidinyl-
43, **53**: n = 4, NR_2 = Morpholinyl-

Scheme 3 General synthetic route for the target ligands **44–53**. Reagents and conditions: (i) (a) pyridine, DMF, rt, 16 h, (b) $NaHCO_{3(aq)}$, 38–90%; (ii) 0.5 M HCl/CH_3OH, rt, 4 h, 65–95%.

(5′-*FAM*-TATAGCTATATTTTTTTATAGCTATA-TAMRA-3′), where *FAM* is the fluorophore donor (6-carboxyfluorescein) and *TAMRA* is the fluorophore acceptor (6-carboxy-*N*,*N*,*N*′,*N*′-tetramethylrhodamine).

Table 1 shows the effect of three different concentrations of compounds **44–49**, **51**, **53** and the known G4 binder RHPS4 (ref. 16) (Fig. 2) on the melting temperature ($\Delta T_{1/2}$) of the labeled oligomers F21T, *c-kit2*, Hsp90a and F10T, respectively.

The data show that ligands **44–49**, **51** and **53** show a moderate ability to stabilize G-quadruplexes. Though most values are appreciably smaller than those for RHPS4, they are still significant in the sense that they allow us to evaluate relative affinities and trends. The ligands with aminoacetyl **44–46** ($n = 1$) are poor G-quadruplex stabilizers, the reason might be that the short side-chains impede effective positioning of the protonated amine in the sugar-phosphate backbone loops, or simply do not provide sufficient surface area for the ligand to bind to the G-quadruplex. The morpholino ligands **45**, **48**, **51** and **53** showed no significant G-quadruplex stabilization, which might result from reduced electrostatic interactions in the backbone and grooves by the uncharged morpholine moiety. For example, the presence of diethylamino group (ligand **47**) and piperidino group (ligand **49**) in place of morpholino group of the inactive ligand **48**, significantly improved the biochemical properties and the binding affinity of **47** and **49** towards the three types of G-quadruplexes.

The results indicated that ligands **47** and **49** induce significant stabilization ($\Delta T_{1/2} > 3.50$ °C) of the three types of G-quadruplex structures at 5.0 μM concentration, with particular affinity for the quadruplex formed by the Hsp90a promoter

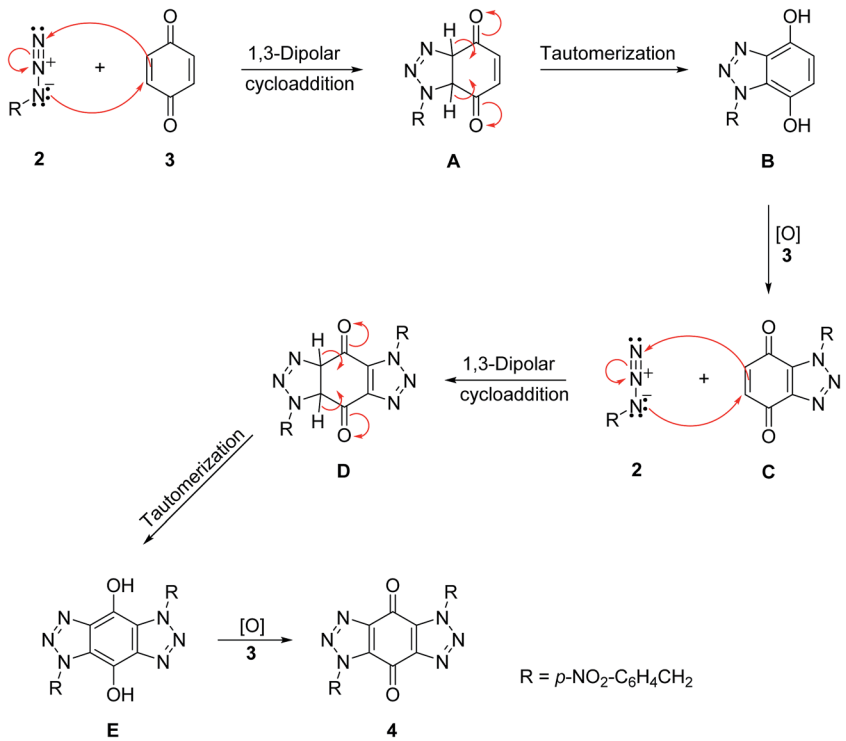

Scheme 4 A mechanism for the formation of bis-triazole **4**.[21,22]

Table 1 $\Delta T_{1/2}$ (°C) data for the compounds **44–49**, **51**, **53** and RHPS4 with telomeric, *c-Kit2*, Hsp90a G4-DNAs and duplex DNA using FRET assay. The yellow highlights represent ligands that show significant binding affinity to the telomeric G-quadruplex, while the green highlight represents the known G4 binder in the literature RHPS4

Ligand	n	HNR_2	F21T				*c-Kit2*				Hsp90A				F10T		
			$T_{1/2}$ (°C)	$\Delta T_{1/2}$ (°C) ± S.D.E.			$T_{1/2}$ (°C)	$\Delta T_{1/2}$ (°C) ± S.D.E			$T_{1/2}$ (°C)	$\Delta T_{1/2}$ (°C) ± S.D.E			$T_{1/2}$ (°C)	$\Delta T_{1/2}$ (°C) ± S.D.E	
			Oligo (0.2 μM)	2.0 μM	3.0 μM	5.0 μM	Oligo (0.2 μM)	2.0 μM	3.0 μM	5.0 μM	Oligo (0.2 μM)	2.0 μM	3.0 μM	5.0 μM	Oligo (0.2 μM)	2.0 μM	5.0 μM
44	1	Dimethylamine	51.9 ± 1.7	-1.0 ± 2.0	-0.7 ± 2.2	1.2 ± 1.9	45.2 ± 2.3	-0.3 ± 3.7	-1.3 ± 3.7	0.7 ± 3.1	49.3 ± 0.7	-0.4 ± 1.3	-0.2 ± 1.5	-0.2 ± 1.3	50.9 ± 1.3	-1.0 ± 1.5	-0.8 ± 1.4
45	1	Morpholine	50.9 ± 0.3	-0.3 ± 1.7	0.2 ± 0.8	3.2 ± 2.5	40.6 ± 0.8	1.9 ± 0.8	3.3 ± 1.1	3.2 ± 0.9	49.8 ± 0.7	-0.5 ± 0.8	-0.1 ± 0.8	0.1 ± 1.0	51.0 ± 0.3	0.2 ± 0.6	0.2 ± 0.3
46	1	Piperidine	50.4 ± 1.4	-0.3 ± 1.8	-0.5 ± 1.7	0.5 ± 1.5	42.2 ± 0.9	-1.9 ± 1.6	-1.6 ± 0.9	0.9 ± 1.3	49.7 ± 0.0	-0.3 ± 0.3	-0.8 ± 0.2	0.3 ± 0.6	51.6 ± 0.3	-0.6 ± 0.7	-0.8 ± 0.4
47	2	Diethylamine	50.4 ± 0.5	2.0 ± 0.6	2.5 ± 1.7	5.6 ± 1.7	42.6 ± 0.3	1.8 ± 0.8	1.8 ± 0.8	4.0 ± 0.8	50.0 ± 0.4	1.5 ± 0.8	3.1 ± 0.5	8.4 ± 0.7	51.9 ± 0.3	0.6 ± 0.8	1.0 ± 0.4
48	2	Morpholine	50.1 ± 0.6	-0.4 ± 1.1	-0.4 ± 0.8	0.0 ± 1.5	43.1 ± 0.4	0.1 ± 0.6	0.4 ± 1.3	0.8 ± 0.5	50.1 ± 0.2	-1.0 ± 0.4	-0.9 ± 0.5	-0.7 ± 0.4	51.5 ± 0.0	-0.8 ± 0.0	-0.7 ± 0.6
49	2	Piperidine	53.8 ± 0.5	1.2 ± 0.8	1.6 ± 1.1	4.5 ± 1.1	45.2 ± 1.2	0.7 ± 3.3	0.8 ± 3.0	7.6 ± 4.0	50.0 ± 0.0	0.9 ± 0.2	2.4 ± 0.6	10.1 ± 0.8	51.3 ± 0.4	0.1 ± 0.5	2.2 ± 0.8
51	3	Morpholine	51.4 ± 0.6	0.5 ± 1.2	0.5 ± 1.0	1.2 ± 1.4	44.3 ± 0.9	-0.2 ± 0.9	-0.9 ± 1.4	-2.5 ± 0.9	50.5 ± 0.3	-0.1 ± 0.6	-0.1 ± 0.4	0.3 ± 0.3	51.9 ± 0.5	0.2 ± 0.5	0.1 ± 0.8
53	4	Morpholine	50.4 ± 0.3	1.6 ± 1.5	1.4 ± 0.6	2.5 ± 1.6	41.9 ± 1.0	1.3 ± 1.1	0.2 ± 1.0	0.6 ± 1.3	50.4 ± 0.3	0.4 ± 0.5	0.4 ± 0.5	0.8 ± 0.3	51.6 ± 0.3	-0.3 ± 3.0	0.3 ± 0.5
RHPS4	-	-	51.7 ± 0.0	11.1 ± 1.4	2.9 ± 3.6	-1.4 ± 2.1	43.0 ± 0.8	7.8 ± 1.6	8.1 ± 1.0	8.1 ± 1.2	50.3 ± 0.5	28.8 ± 0.6	29.6 ± 0.5	24.9 ± 3.6	51.6 ± 0.5	-0.2 ± 0.6	0.6 ± 0.5

sequence. Therefore, the study reveals the ligands **47** and **49** to be the best binders of the series towards telomeric G4-DNA, and promoter sequences G4-DNA of *c-Kit2* and Hsp90a, respectively, over the concentration range examined. Good selectivity for G-quadruplex DNA *vs.* duplex DNA was displayed by the ten ligands over the concentration range used. None of them were observed to significantly increase the melting temperature of duplex forming strand F10T (ds), suggesting a very low stability for any duplex–ligand complex.

According to the FRET assay results, we find that an increase in length of the side chain by one $-CH_2-$ unit results in a large increase in the ability of the compounds to stabilize G-quadruplex DNA structure. Also, the nature of the amine substituent at the terminus of the side chain greatly affects the ability of the compounds to stabilize quadruplex DNA.

In a number of cases (*e.g.* **47** and **49**), there is a noticeable jump in $\Delta T_{1/2}$ from 3 μM to 5 μM. One possible explanation for this is that these ligands show cooperative binding to the DNA. This would not be unusual for quadruplex binders – *e.g.* cooperativity in binding of RHPS4 to the *c-kit* DNA quadruplex has been detected by mass spectroscopy.[19]

There are a few examples of negative $\Delta T_{1/2}$ values but on the whole they are within experimental error of zero. However a negative $\Delta T_{1/2}$ value is of course quite possible, if the ligand stabilizes some unfolded form of the DNA more strongly than it stabilizes the quadruplex fold.

When comparing the melting temperatures of the eight ligands **44–49**, **51** and **53** with those of the known G-quadruplex binder RHPS4, we notice that all the new ligands are less effective at G-quadruplex stabilization. The key difference between the bis-triazoles series **44–53** and the G4 binders RHPS4 (ref. 16), trisubstituted acridine BRACO-19 (ref. 14) and tetrasubstituted naphthalene diimide BMSG-SH-3 (ref. 12) (Fig. 2) is the presence of the two sp^3 methylene groups within the aromatic region that might perturb the planarity of the hydrophobic aromatic core, and thus affect the π–π staking of the ligands on to the terminal G-quartet. As well as the presence of four hydrophilic arms terminating in protonated piperazine groups and three terminating in protonated pyrrolidine in BMSG-SH-3 and BRACO-19, respectively, increases their electronic interaction with the G4 grooves, in comparison to the bis-triazoles **47** and **49**.

2. Circular dichroism spectroscopy. Circular dichroism spectroscopy[28–30] was used to investigate the interaction of ligand **47** with human telomeric DNA sequences and influence on the G-quadruplex folding topology (parallel or anti-parallel). Parallel G-quadruplexes, where all strands are in the same orientation, give CD spectra with a maximum at 260 nm and a shallow dip at 240 nm. Anti-parallel quadruplexes show a maximum ellipticity at 290 nm and a minimum at 260 nm.[31] We selected ligand **47** for the first CD study as it has the highest affinity for the telomeric G-quadruplex. Since the FRET studies indicated a ligand : DNA ratio of at least 5 : 1 was required to observe significant quadruplex stabilization, stock solutions of bis-triazole **47** and the known binder RHPS4 were added to the 22 base human telomeric G4 oligonucleotide $AGGG(TTAGGG)_3$ (*h*-Tel) in potassium chloride buffer medium to generate solutions of (3.3 μM) *h*-Tel with (16.5 μM) ligand **47** and RHPS4 of the ratio 1 : 5 of DNA to ligand, (1.0 μM) of *h*-Tel with (15.0 μM) of ligand **47** and RHPS4 of the ratio 1 : 15 of DNA to ligand, and (1.0 μM) of *h*-Tel with (25.0 μM) of ligand **47** and RHPS4 of the ratio 1 : 25 of DNA to ligand.

The CD spectrum (Fig. 3) of the native *h*-Tel (red line) shows a strong positive band at 290 nm, with a small minimum at 235 nm and a number of additional broad positive bands apparent at 250 nm and 275 nm. This spectrum is likely to correspond to a mixture of parallel and anti-parallel folds possibly including hybrid forms as well.[8,19,31,32] The CD spectra **A**, **B** and **C** show that the G-quadruplex topology of *h*-Tel is retained on binding to ligand **47**, with minor changes in the spectra (green line) being apparent, indicating that **47** does not

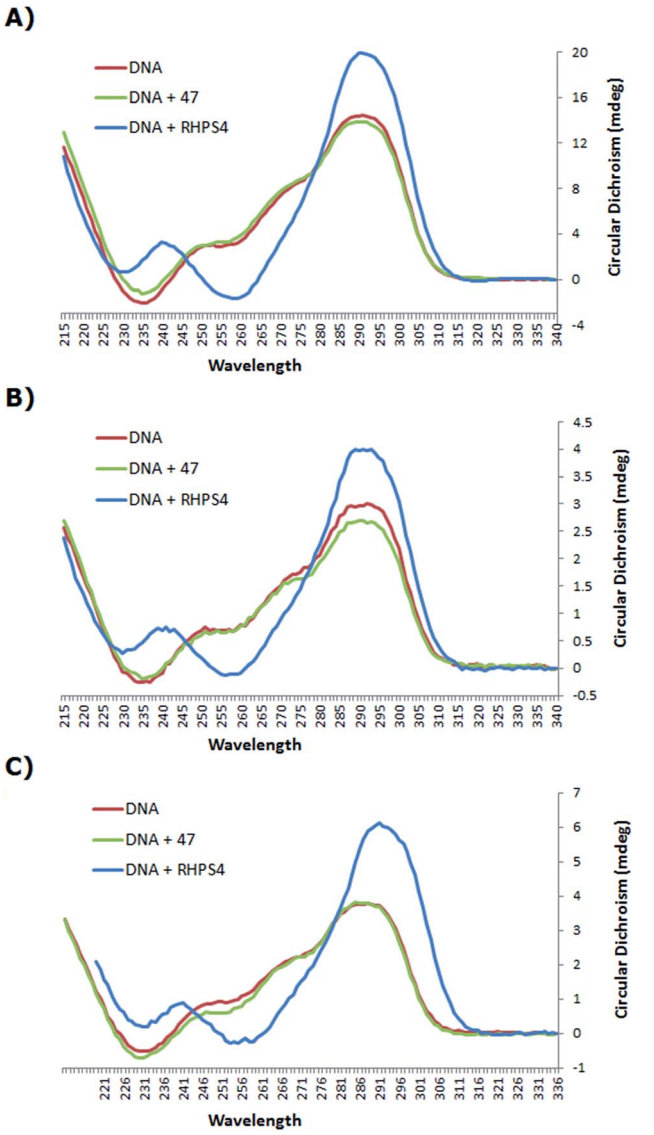

Fig. 3 CD spectra of *h*-Tel and the complexes with ligand **47** and RHPS4 in potassium chloride buffered to pH = 7.0, at 25 °C, (A) 3.3 μM of *h*-Tel with 16.5 μM of ligand **47** and RHPS4 (of the ratio 1 : 5 of DNA to ligand); (B) 1.0 μM of *h*-Tel with 15.0 μM of ligand **47** and RHPS4 (of the ratio 1 : 15 of DNA to ligand); (C) 1.0 μM of *h*-Tel with 25.0 μM of ligand **47** and RHPS4 (of the ratio 1 : 25 of DNA to ligand).

induce major changes in telomeric topology on binding. In contrast, binding of RHPS4 (blue line) induces major changes in the CD spectra that are interpreted as almost complete conversion to the anti-parallel-stranded topology. These results suggest that, compared to RHPS4, **47** is a relatively promiscuous G-quadruplex ligand, and/or that CD spectroscopy is not sensitive enough to clearly resolve the topological dependence in the relatively weak binding affinity of ligand **47** – compared to RHPS4 – towards the human telomeric G4 structure, (shown by the FRET melting assay). Because ligand **47**, our best telomeric G4 stabilizer, proved not to have a detectable influence on the topology of the quadruplex (parallel *versus* antiparallel form), we did not consider it of value to investigate other, structurally related but lower affinity, ligands such as **49**.

3. Molecular modeling. In order to gain insight into the nature of the ligand–DNA interactions, and help rationalize the FRET melting data, a series of molecular modeling studies was performed. The synthesized bis-triazoles **44–53** were docked to the human telomeric parallel stranded (propeller-like) G-quadruplex DNA crystal structure (PDB ID 1KF1),[8] at both 3′- and 5′-sides, using the Glide software package.[33,34] We used the parallel structure as a template for modeling studies rather than any of the anti-parallel forms obtained from NMR studies because of the relatively inconclusive FRET data, the fact that its topology is such that guanine tetrads at both 3′- and 5′-sides are potential binding sites for ligands,[35] and in addition because the parallel structure is considered to be biologically more relevant due to the higher intracellular concentration of K^+.[8,31] Furthermore, the structures of the synthesized bis-triazoles **44–53** are quite similar to that of the known binder TRZ which stabilizes the parallel human G4 structure selectively.[19]

In analysing the docking data, we concentrated on high-scoring poses that were conserved across all members of the congeneric set of ligands, in order to investigate and explore the binding interactions between the ligands and G4-DNA.

The study showed that all the ligands should have affinity for both 3′- and 5′-faces of the human telomeric parallel standard G-quadruplex DNA structure. Fig. 4 shows the VMD top views of the 3′-face of the telomeric parallel G-quadruplex DNA template, and the set of ligands **44–53** bound to the 3′-side of G4-DNA in the best pose for their common core. Despite differences in the sidechains, the majority of the ligands bound in a very similar fashion with only minor variations in some intermolecular interactions between models. Furthermore, all the ligands were oriented and posed with the 3′-face in fashions that agree with the accepted requirements for the stabilization of G-quadruplex structures; the ligands' hydrophobic aromatic cores are positioned over the external G-quartet and their hydrophilic amino side arms are directed into the grooves and TTA loops of the telomeric G4-DNA, as shown in the VMD top views (Fig. 4B).

In order to gain insight into the nature of interactions between synthesized bis-triazoles **44–53** and the 3′-side of the telomeric parallel G-quadruplex, the side view of the common pose for ligand **47** (the best binder of the series) with 3′-face was studied closely. The side view in VMD (Fig. 5) shows that the aromatic core of ligand **47** does not stack perfectly over the external guanine tetrad, resulting in weak π–π interactions between the

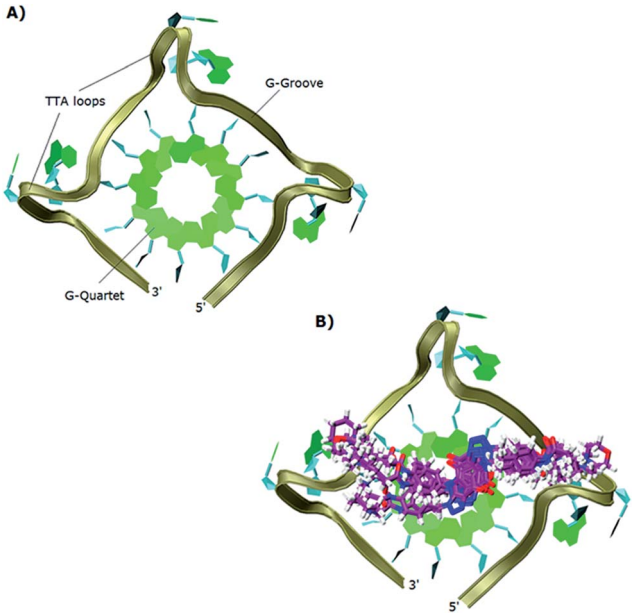

Fig. 4 Top views in VMD visualizing software of: (A) 3′-side template of the telomeric parallel G4-DNA; (B) the common pose for ligands **44–53** with the 3′-side of G4-DNA.

two. This explains and rationalizes the moderate binding affinity the ligands revealed by the FRET melting data ($\Delta T_{1/2}$). The main reason for this ineffective stacking is the presence of the two sp^3 methylene groups within the aromatic region which perturb the planarity of the hydrophobic aromatic core. The side view also shows the amide nitrogen and the tertiary amine functionality at the ends of the side chains both contribute towards stabilization of the complex by forming hydrogen bonds to phosphate groups of one groove and two TTA loops. Furthermore, the presence of a positive charge on the protonated tertiary amino group would enhance the electrostatic interactions with the negatively charged phosphate groups in the loops.

Similar results were obtained from docking the bis-triazoles **44–53** to the 5′-side of G4-DNA template: a high-scoring "consensus" pose is found in which the benzoquinone core stacks appreciably, but sub-optimally, with the G-quadruplex face and the side chains orient to find favourable electrostatic binding opportunities in the sugar–phosphate grooves and loops.

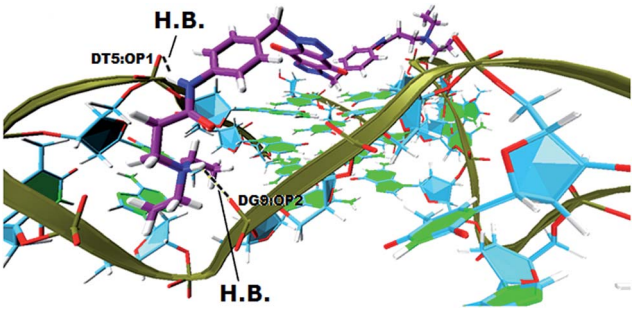

Fig. 5 A side view of ligand **47** with the 3′-side G4 template (hydrogen bonds in yellow lines).

4. Cell biology studies. The anti-proliferative activities of the eight bis-triazoles **44–53** plus the known G-quadruplex binder RHPS4 (ref. 16) were evaluated *in vitro* using the MTT assay[36,37] against human carcinoma HCT-116 (colorectal) and MiaPaCa-2 (pancreatic) cell lines, and also human MRC-5 (embryonic lung fibroblasts) to investigate their selective cytotoxicity. Colorectal carcinoma is the third most common cancer and caused more than 600 000 deaths globally in 2008.[38] Pancreatic carcinoma is particularly resistant to chemotherapy, often diagnosed with metastatic disease and has an appalling five year survival rate (<5%).[39] Thus, the development of new therapies for such malignant diseases represents a current unmet medical need.

Concentrations at which cell growth is inhibited by 50% (GI_{50}) after 72 h exposure of cells to bis-triazoles **44–53** and RHPS4 were calculated from dose–response curves and are presented in Table 2. RHPS4 structure is shown in Fig. 2.

As can be seen from Table 2, most of the compounds **44–49**, **51**, **53** and RHPS4 show potent cellular growth inhibitory activity against both carcinoma cell lines in the concentration range (0.01–100 μM) used. The highest potency against human cancer cell lines is shown by the ligand **44** (a non G4 binder) with GI_{50} values of 70 nM for HCT-116 and 60 nM for MiaPaCa-2, ligand **46** (a non G4 binder) which has a GI_{50} value of 70 nM for HCT-116, and our best *c-Kit2* and Hsp90a G4 binder **49** which shows GI_{50} values of 80 nM for HCT-116 and 60 nM for MiaPaCa-2. The three compounds show almost identical activity with uniform growth inhibitory responses by the two cancer cell lines HCT-116 and MiaPaCa-2 (except **46**). We see that ligand **47**, the potent telomeric G4 stabilizer, has relatively lower anti-proliferative activity against both human cancer cell lines. This strongly suggests that the synthesized bis-triazoles **44–49**, **51**, **53** perturb molecular targets other than the telomere, and mechanisms of action in addition to G-quadruplex binding may contribute to antitumour activity.

The results show that the eight synthesized ligands have higher potencies against the human cancer cell lines HCT-116 and MiaPaCa-2 than in normal human lung MRC-5 fibroblasts, inferring good selectivity in their cellular growth inhibitory activity for human cancer cells over human normal cells. These results suggest **44–53** have promise as new therapeutic anticancer agents.

Table 2 Growth inhibitory activity of compounds **44–49**, **51**, **53** and RHPS4 against human cancer HCT-116 and MiaPaCa-2 and normal MRC-5 cell lines. GI_{50} values are represented as mean ± standard error of mean (SEM) of at least two independent experiments (n = 8 per trial). The yellow highlights represent the most potent ligands against the three types of cell lines, while the green highlight represents the known G4 binder in the literature RHPS4

Compound	n	H-NR_2	GI_{50} (μM) ± S.E.M		
			HCT-116 cell line (Colon cancer)	MiaPaCa-2 cell line (Pancreatic cancer)	MRC-5 cell line (Lung normal)
44	1	Dimethylamine	0.07 ± 0.01	0.06 ± 0.04	0.6 ± 0.1
45	1	Morpholine	0.6 ± 0.1	1.3 ± 0.6	4.1 ± 1.8
46	1	Piperidine	0.07 ± 0.04	0.2 ± 0.01	1.2 ± 1.1
47	2	Diethylamine	0.3 ± 0.01	0.3 ± 0.02	2.2 ± 0.8
48	2	Morpholine	2.9 ± 0.5	13.0 ± 15.0	69.5 ± 2.0
49	2	Piperidine	0.08 ± 0.01	0.06 ± 0.02	1.3 ± 0.1
51	3	Morpholine	1.9 ± 0.9	2.3 ± 0.04	28.7 ± 19.6
53	4	Morpholine	0.6 ± 0.1	0.6 ± 0.2	1.2 ± 0.6
RHPS4	-	-	5.7 ± 1.1	5.5 ± 0.6	9.7 ± 1.3

In particular, the results indicate that compound **49** is >16-fold more active against cancer human cell lines HCT-116 and MiaPaCa-2 than against normal human MRC-5 cells. Compared to RHPS4, **49** is both more potent against the two tumour cell lines (GI_{50} values $\leq$ 0.08 mM) and more selective for them over MRC-5.

Conclusions

In conclusion, the design, synthesis, biophysical and biological evaluation of a new series of bis-triazoles **44–53** as potential G-quadruplex stabilizers have been described. The target ligands can be obtained through an efficient, convergent, synthetic route in moderate to good yields. In FRET assays two ligands show significant binding to the three types of G-quadruplex structures with selectivity towards the promoter sequence of the Hsp90a oncogene. The synthesized bis-triazoles **44–49**, **51** and **53** are selective towards G4-DNA *vs.* duplex-DNA. The planarity of the aromatic core, number of the hydrophilic side arms and the nature of the amino group at their termini greatly affect the ability of the compounds to stabilize the G-quadruplex. Circular dichroism-based studies of the topology of the human telomeric G-quadruplex obtained from its interaction with ligand **47** suggest that both parallel and anti-parallel folds might be present. In MTT assays, most of the synthesized ligands show potent cell growth inhibitory activity against human carcinoma (colon and pancreatic) cell lines. Notably they are more potent towards human cancer cells than embryonic lung fibroblasts. The weak correlation between FRET and MTT assay results suggests that the synthesized ligands may have additional mechanisms of action besides targeting G-quadruplexes.

Docking studies give us a clear idea about the nature of the ligand–quadruplex DNA interactions and rationalize the moderate binding affinity the ligands show in the FRET experiments, suggesting that the hydrophobic core is not planar enough for optimal π–π stacking interactions between the aromatic portion of the ligands and the external G-quartet. This information can guide the optimization of ligands **44–53**, for increased binding affinity and selectivity toward G-quadruplex structures.

Experimental section

FRET analysis

All oligonucleotides and their fluorescent conjugates were purchased from Sigma. DNA was initially dissolved as a stock 100 μM solutions in purified water; further dilutions were carried out in the relevant buffer. The ability of the compounds to stabilize G-quadruplex DNA was investigated using a fluorescence resonance energy transfer (FRET) assay modified to be used as a high-throughput screen in a 96-well format. The dual labeled oligonucleotides F21T (5′-*FAM*-GGGTTAGGGT TAGGGTTAGGG-*TAMRA*-3′), *c-kit2* (5′-*FAM*-CCCGGGCGG GCGCGAGGGAGGGGAGG-*TAMRA*-3′) and Hsp90a (5′-*FAM*-GGGCCAAAGGGAAGGGGTGGG-*TAMRA*-3′); donor fluorophore *FAM*: 6-carboxyfluorescein; acceptor fluorophore *TAMRA*: 6-carboxy-*N*,*N*,*N*′,*N*′-tetramethylrhodamine used as the FRET probes, were diluted from stock to the correct concentration (0.2 μM) in a 60 mM potassium cacodylate buffer (pH 7.4) and then annealed by heating to 95 °C for 10 min, followed by cooling to room temperature in the heating block for 3.5 h. An analogous protocol was used in the preparation of the labeled hairpin DNA for experiments assessing the duplex-stabilizing interactions of the compound. The oligonucleotide used (F10T) was purchased as the dual-labeled probe forming the palindromic decamer sequence d(TATAGCTATA) with T_6 between two sequences to make the hairpin loop (5′-*FAM*-TATAGCTATATTTTTTTA TAGCTATA-TAMRA-3′) and annealed under the same conditions as the other oligonucleotides. Compounds were stored at −20 °C as 1 mM stock solutions in a mixture of hydrochloric acid (75% 1 mM HCl and 25% purified water) and DMSO (9 : 1), after which 60 mM potassium cacodylate buffer (pH 7.4) was used in all subsequent steps. All experimental values were determined in triplicate. 96-well polypropylene plates (Agilent Technologies) were prepared by aliquoting 50 μL of the annealed DNA into each well, followed by 50 μL of compound solutions.[1,25] Measurements were made on a real-time PCR apparatus[40] (MX3005P, Stratagene) with excitation at 450–495 nm and detection at 515–545 nm. Fluorescence readings were taken at intervals of 0.5 °C over the range 25–99 °C for 148 cycles, with a constant temperature being maintained for three minutes at 25 °C and 30 seconds prior to each reading to ensure a stable value. Final analysis of the data was carried out using a Microsoft Excel 2010. Esds in $\Delta T_{1/2}$ are ±4.0 °C. In brief, for the determination of the melting temperature, the raw data from the fluorescence detector was analysed by two ways: (i) normalizing the fluorescein emission between 0 and 1, then calculating the temperature for which the normalized emission equals to 0.5 which is defined as $T_{1/2}$, and the normalized melting curve was plotted as normalized fluorescein emission *vs.* compound concentration; (ii) the fluorescein emission data were first smoothed using 8-point running average, subsequently the first derivative of the smoothed data was calculated, then the temperature that matches the maximum of the first derivative is determined which is defined as T_{max}. The first derivative melting curve was plotted as d(fluorescein emission)/dT *vs.* compound concentration.[26]

CD spectroscopy

CD and UV spectra of *h*-Tel oligonucleotides were recorded on an Applied Photophysics Chirascan plus spectrophotometer interfaced with Chirascan software. The optical system consisted of a 150 W ozone producing xenon lamp, circular light polarizer and end-mounted photomultiplier. Temperature regulation was performed using a Poly Science water bath and Quantum Northwest TC125 controller. Calibration was performed prior to these experiments with D-camphorsulfonic acid. Data were recorded in a 1 cm path length quartz cuvette containing 3 mL samples. Bandwidth was set to 1.0 nm for entrance and exit, and data was recorded with steps of 1 nm over the wavelength range 340–215 nm. The number of samples was set to 100 000 for CD and 10 000 for UV with adaptive sampling enabled. Each reported curve is the average of 3 repeat scans.

The oligonucleotide 5′-AGGGTTAGGGTTAGGGTTAGGG-3′ (*h*-Tel) was supplied lyophilized and purified by desalting by

Sigma. Dilution of the lyophilized sample was performed using 100 mM potassium chloride and 10 mM potassium phosphate buffer solution at pH 7.0. The concentration of DNA stock solution was determined using molar extinction coefficient 228 500 mol^{-1} cm^{-1} at a UV maximum of 260 nm. Compounds to be tested for interaction with *h*-Tel were dissolved in methanol to make a 2.0 mM solution. Solutions of 1.0 and 3.3 μM *h*-Tel in potassium chloride buffer were annealed by heating to 95 °C for 10 minutes before being allowed to slowly cool to ambient temperature over 4 hours, with or without the addition of a ligand at ratios of 1 : 5, 1 : 15 and 1 : 25 DNA to ligand concentration. Analysis of data was performed using Microsoft Excel. Baseline data was collected using buffer solution in the same cuvette and subtracted from sample spectra, after which the data was normalized to zero at 340 nm.[28,41]

MTT assay

The antiproliferative activity of experimental agents was evaluated by MTT [3-(4,5-dimethylthiazol-2-yl)-2,5-diphenyl tetrazolium bromide] assay[36] on 3 different human cell lines: colon (HCT-116) and pancreatic (MiaPaCa-2) carcinoma, and embryonic lung fibroblasts (MRC-5). Cell lines were sourced from the American Type Culture Collection (ATCC) and stored in liquid nitrogen. Low passage numbers (≤20) were used in all experiments. Lonza MycoAlert™ mycoplasma detection kits were used (according to manufacturer's instructions) ensuring cultures were contamination-free. The carcinoma cell lines were maintained in RPMI-1640 (Sigma-Aldrich (UK), CN: R8758) medium supplemented with 10% (v/v) heat-inactivated fetal bovine serum (FBS). MRC-5 fibroblasts were maintained in Minimum Essential Medium (MEM) Eagle (Sigma-Aldrich (UK), CN: M0275) supplemented with 10% (v/v) FBS, 1% sodium carbonate (7.5%), 1% non-essential amino acids (0.1 mM), 1% HEPES (1 M), 1% L-glutamate (200 mM) and 1% penicillin. The cells were seeded into 96-well plates at density of 3×10^3 per well (180 μL per well) and allowed to adhere for 24 h at 37 °C/5% CO_2. Agent top stock solutions (10 mM in DMSO) were then freshly made. Serial dilutions were prepared in the same media as mentioned above for addition to carcinoma and normal cells. Control wells received vehicle alone (20 μL per well). Final test agent concentrations in the wells were; 0.01, 0.05, 0.1, 0.5, 1, 5, 10, 50 and 100 μM. The final concentration of DMSO in the wells never exceeded 1%. Vehicle control assays were performed (0.0001–1% DMSO). Experimental plates were incubated for a further 72 h period at 37 °C/5% CO_2. Cell viability was recorded at the time of agent addition (T_0) and after 72 h exposure: following addition of MTT solution (2 mg mL^{-1} in PBS: 50 μL per well), experimental plates were incubated for 3 h to allow reduction of MTT by viable cells to insoluble dark purple formazan crystals. The supernatant in each well was then aspirated, and cellular formazan was solubilized by addition of DMSO (150 μL per well). Absorbance was read at a wavelength of 550 nm by using an Anthos Labtec systems plate reader. The measured intensity is proportional to metabolic activity, which correlates with viable cell numbers. Estimated GI_{50} values (test agent concentrations that inhibit cell growth by 50%) were calculated.[39]

Molecular docking studies

1. **Preparation of DNA and ligands.** The crystal structure of the 22-mer parallel-standard propeller-loop topology (PDB 1KF1: resolution 2.10 Å) human telomeric G-quadruplex[8,35] was obtained from the Protein Data Bank and used as a starting point to examine plausible interactions with the ligands. Using the Maestro programme (in Schrodinger package), the terminal 5′ adenine residue was removed to generate 21-mer structure, so the flat planar quartet is exposed to the ligand. Using "Protein Preparation" tools in Glide software[34] (built in Maestro), water molecules were removed from the structure file, missing hydrogen atoms were added, non-polar hydrogens merged to their corresponding carbons, bond orders were assigned and potassium ions were deleted because we expect their effect to be almost independent of the ligand, and so not contributing to selectivity. The molecular models for the bis-triazoles series of ligands were constructed, minimized, partial charges were calculated, atomic names and bond orders were assigned using Maestro program.

2. **Receptor grid generation and docking protocol.** The receptor grid map representing G-quadruplex DNA was calculated and generated using "Glide Generation" option in "Docking" tools of Glide software. The grid was chosen to encompass the entire DNA molecule, such that it fits to docked ligands with length of ≤36 Å. The size of the entire green small box around the external G-quartet of the G4-DNA is 14 Å × 14 Å × 14 Å.

The automated docking studies were carried out using "Glide docking" tools of Glide software, which uses the ChemScore function of Eldridge *et al.*[42] to calculate Glide docking scores. The programme ran 10 000 docking trials per ligand, and wrote out at most 50 poses for each ligand.

Chemistry

Details of all synthetic procedures are included in the ESI.†

PDB ID code

The PDB ID code for the published telomeric parallel G-quadruplex DNA structure is 1KF1.

Conflicts of interest

There are no conflicts to declare.

Abbreviations

CD	Circular dichroism
c-Kit2	Labelled G-quadruplex forming oligomer of the promoter sequence *c-kit2* oncogene
FAM	6-(Carboxylfluorescein)
FRET	Fluorescence resonance energy transfer
F10T	Hairpin double helix forming labeled oligomer
F21T	Labeled G-quadruplex forming oligomer of human telomeric sequence

GI_{50}	Concentration inhibiting 50% cell growth
Glide	Grid-based ligand docking with energetic
HCT-116	Human colorectal carcinoma cell line
Hsp90a	Labeled G-quadruplex forming oligomer of the promoter sequence Hsp90a oncogene
MiaPaCa-2	Human pancreatic carcinoma cell line; MRC-15 embryonic lung fibroblast cell line
MTT	3-(4,5-Dimethylthiazol-2-yl)-2,5-diphenyl tetrazolium bromide
OD	Optical density
TAMRA	6-Carboxytetramethylrhodamine
VMD	Visual molecular dynamics

Acknowledgements

We thank the Islamic Development Bank (IDB) in Jeddah/KSA for financial support. We are grateful to Prof. Steven Neidle and Dr Cristina Ciancimino from University College of London (UCL) for their help in using the FRET assay, Dr Abigaill Emtage from University of Nottingham/Malaysia Campus for her advice in using Glide program, and Prof. Mutasem Taha from Jordan University for his guidance and scientific advice about targeting telomere and telomerase.

References

1 A. D. Moorhouse, S. Haider, M. Gunaratnam, D. Munnur, S. Neidle and J. E. Moses, *Mol. BioSyst.*, 2008, **4**, 629–642.
2 N. J. Elwood, *Cancer Control*, 2004, **11**, 77–85.
3 L. K. Wai, *Medsc. Gen. Med.*, 2004, **6**, 19–29.
4 A. M. Olovinkov, *Dokl. Akad. Nauk SSSR*, 1971, **201**, 1496–1499.
5 A. M. Olovnikov, *J. Theor. Biol.*, 1973, **41**, 181–190.
6 A. De Cian, L. Lacroix, C. Douarre, N. Temime-Smaali, C. Trentesaux, J.-F. Riou and J.-L. Mergny, *Biochimie*, 2008, **90**, 131–155.
7 R. Pruzan, K. Pongracz, K. Gietzen, G. Wallweber and S. Gryaznov, *Nucleic Acids Res.*, 2002, **30**, 559–568.
8 G. N. Parkinson, M. P. H. Lee and S. Neidle, *Nature*, 2002, **417**, 876–880.
9 Y. Xu, T. Ishizuka, K. Kurabayashi and M. Komiyama, *Angew. Chem., Int. Ed.*, 2009, **48**, 7833–7836.
10 L.-P. Bai, M. Hagihara, K. Nakatani and Z.-H. Jiang, *Sci. Rep.*, 2014, **4**(6767), 1–10.
11 N. H. Campbell, M. Patel, A. B. Tofa, R. Ghosh, G. N. Parkinson and S. Neidle, *Biochemistry*, 2009, **48**, 1675–1680.
12 M. Gunaratnam, M. de la Fuente, S. M. Hampe, A. K. Todd, A. P. Reszka, A. Schätzlein and S. Neidle, *Bioorg. Med. Chem.*, 2011, **19**, 7151–7157.
13 D. Monchaud and M.-P. Teulade-Fichou, *Org. Biomol. Chem.*, 2008, **6**, 627–636.
14 M. J. B. Moore, C. M. Schultes, J. Cuesta, F. Cuenca, M. Gunaratnam, F. A. Tanious, W. D. Wilson and S. Neidle, *J. Med. Chem.*, 2006, **49**, 582–599.
15 K. Shin-ya, K. Wierzba, K.-i. Matsuo, T. Ohtani, Y. Yamada, K. Furihata, Y. Hayakawa and H. Seto, *J. Am. Chem. Soc.*, 2001, **123**, 1262–1263.
16 E. Gavathiotis, R. A. Heald, M. F. G. Stevens and M. S. Searle, *J. Mol. Biol.*, 2003, **334**, 25–36.
17 J. L. Mergny, L. Lacroix, M. P. Teulade-Fichou, C. Hounsou, L. Guittat, M. Hoarau, P. B. Arimondo, J. P. Vigneron, J. M. Lehn, J. F. Riou, T. Garestier and C. Helene, *Proc. Natl. Acad. Sci. U. S. A.*, 2001, **98**, 3062–3067.
18 I. M. Dixon, F. Lopez, A. M. Tejera, J.-P. Esteve, M. A. Blasco, G. Pratviel and B. Meunier, *J. Am. Chem. Soc.*, 2007, **129**, 1502–1503.
19 T. P. Garner, H. E. L. Williams, K. I. Gluszyk, S. Roe, N. J. Oldham, M. F. G. Stevens, J. E. Moses and M. S. Searle, *Org. Biomol. Chem.*, 2009, **7**, 4194–4200.
20 X.-L. Wang, K. Wan and C.-H. Zhou, *Eur. J. Med. Chem.*, 2010, **45**, 4631–4639.
21 S. T. Abu-Orabi, M. Saleh, L. Al-Momani, I. Jibril and Y. Yousef, *Jordan J. Chem.*, 2006, **1**, 109–120.
22 M. Saleh, Master, Yarmouk University, 2000.
23 C. Marminon, J. Gentili, R. Baret and P. Nebois, *Tetrahedron*, 2007, **63**, 735–739.
24 H. Devarajan-Ketha and K. B. Sloan, *Bioorg. Med. Chem. Lett.*, 2011, **21**, 4078–4082.
25 D. Renciuk, J. Zhou, L. Beaurepaire, A. Guedin, A. M. Bourdoncle and J.-L. Mergny, *Methods*, 2012, **57**, 122–128.
26 A. D. Cian, L. Guittat, M. Kaiser, B. Saccà, S. Amrane, A. Bourdoncle, P. Alberti, M.-P. Teulade-Fichou, L. Lacroix and J.-L. Mergny, *Methods*, 2007, **42**, 183–195.
27 J.-L. Mergny, *Biochemistry*, 1999, **38**, 1573–1581.
28 R. W. Woody, *Methods Enzymol.*, 1995, **246**, 34–71.
29 W. C. Johnson, *Protein Struct. Funct. Genet.*, 1990, **7**, 205–214.
30 G. D. Fasman, *Circular dichroism and conformational analysis of biomolecules*, Springer, 1996.
31 A. Ambrus, D. Chen, J. Dai, T. Bialis, R. A. Jones and D. Yang, *Nucleic Acids Res.*, 2006, **34**, 2723–2735.
32 A. T. Phan, V. Kuryavyi, K. N. Luu and D. J. Patel, *Nucleic Acids Res.*, 2006, **35**, 6517–6525.
33 R. A. Friesner, J. L. Banks, R. B. Murphy, T. A. Halgren, J. J. Klicic, D. T. Mainz, M. P. Repasky, E. H. Knoll, M. Shelley, J. K. Perry, D. E. Shaw, P. Francis and P. S. Shenkin, *J. Med. Chem.*, 2004, **47**, 1739–1749.
34 L. L. C. Schrodinger, *The Glide 2.5 calculations used First Discovery, version 2.5021*, New York, June 2003.
35 G. N. Parkinson, R. Ghosh and S. Neidle, *Biochemistry*, 2007, **46**, 2390–2397.
36 T. Mosmann, *J. Immunol. Methods*, 1983, **65**, 55–63.
37 F. Denizot and R. Lang, *J. Immunol. Methods*, 1986, **89**, 271–277.
38 K. R. Bauer, M. Brown, R. D. Cress, C. A. Parise and V. Caggiano, *Cancer*, 2007, **109**, 1721–1728.
39 M. Cini, T. D. Bradshaw, W. Lewis and S. Woodward, *Eur. J. Org. Chem.*, 2013, 3997–4007.
40 R. A. J. Darby, M. Sollogoub, C. McKeen, L. Brown, A. Risitano, N. Brown, C. Barton, T. Brown and K. R. Fox, *Nucleic Acids Res.*, 2002, **30**, e39.
41 A. Patel, W. Lewis, M. S. Searle, M. F. G. Stevens and C. J. Moody, *Tetrahedron*, 2015, **71**, 7339–7343.
42 M. D. Eldridge, C. W. Murray, T. R. Auton, G. V. Paolini and R. P. Mee, *J. Comput.-Aided Mol. Des.*, 1997, **11**, 425–445.

